Element Mapping of the Esquel Pallasite by Micro X-ray Fluorescence Analysis

Chun-Jung Chen

Department of Geology, National Museum of Natural Science, Taichung 404, Taiwan

(Received December 12, 2023; Accepted December 21, 2023; Published online February 26, 2024)
DOI:10.6693/CAR.202401_(36).0004

Abstract. A large slab of the Esquel pallasite was characterized by micro X-ray fluorescence (μ-XRF) analysis for the first time. Element mapping of the Esquel pallasite highlighted that (1) the phase abundances (in vo1%) are olivine (58%), kamacite (26%), taenite (10%), troilite (1.7%), schreibersite (1.5%), chromite (0.7%) and phosphates (1.5%; such as merrillite or stanfieldite); and (2) the olivine chemical composition varies in terms of trace elements such as Mn, As, and Zn. The coexistence of angular olivines and olivine aggregates, along with variations in trace elements such as manganese, zinc, and arsenic within olivine, indicates that the Esquel pallasite meteorite underwent multiple stages, potentially involving one or multiple impact events during its formation process.

Key words: pallasite, Esquel, micro X-ray fluorescence analysis, μ-XRF, element mapping.

INTRODUCTION

Pallasites represent a subclass of stony-iron meteorites predominantly characterized by olivine ($(Mg,Fe)_2SiO_4$) contents ranging 35%–85% by volume (Weisberg *et al*. 2006). The residual portion consists mainly of metallic phases primarily composed of (Fe, Ni) metal. These primary phases exhibit distinct physical and geochemical characteristics, classifying pallasites within the differentiated meteorite group (Norton and Chitwood 2008). Olivines within pallasites display uniform textures and compositions within individual samples, occasionally demonstrating slight enrichments in either Fe or Mg, known as olivine zoning (Miyamoto 1997). The (Fe, Ni) metal within pallasites forms a connected network, occasionally exhibiting the characteristic Widmanstätten pattern observed in iron meteorites. Three principal constituents form the (Fe, Ni) metal assemblage: kamacite (with Ni concentrations ranging 4–7.5 wt%), taenite (with Ni contents ranging 27–65 wt%), and plessite (a mixture of kamacite and taenite). Kamacite is predominant and often surrounded by taenite lamellae. Minor phases include sulfide troilite (FeS), phosphate minerals such as merrillite ($Ca_{18}Na_2Mg_2(PO)_2$), stanfieldite ($Ca_3Mg_3(PO_4)_4$), and farringtonite ($Mg_3(PO_4)_2$), as well as phosphide schreibersite ($(Fe,Ni)_3P$), chromite ($FeCr_2O_4$), pyroxene (e.g., orthopyroxenes $(Mg,Fe)SiO_3$), and P-rich olivines.

Pallasites are theorized to have originated at the interface between a silicate mantle and a molten metal core within a differentiated asteroid, resulting from impact-induced mingling of olivine-rich mantle fragments and liquid metallic material from the core (Yang *et al*. 2010). Nevertheless, recent investigations indicated that numerous pallasites did not undergo cooling at the core-mantle boundary but instead exhibit cooling patterns consistent with smaller bodies formed from a grazing collision between the

*Corresponding author. E-mail: cjchen618@nmns.edu.tw

initially differentiated asteroid and larger celestial bodies (Yang *et al*. 2010). The specific genesis of pallasite formation remains contentious, with uncertainties surrounding the mechanisms underlying the mixing process between olivine and liquid metal.

Four distinct categories of pallasites exist which are distinguished by variations in their silicate mineralogy, metal composition, and O isotopic compositions, namely (1) Main Group (MG) pallasites, (2) the Eagle Station (ES) grouplet, (3) pyroxene pallasites (Boesenberg *et al*. 1995), and (4) the ungrouped pallasite of Milton (Weisberg *et al*. 2006). Several notable pallasites, like Brenham, Brahin, Esquel, Imilac, Sericho, and Seymchan, are substantial stones, often weighing hundreds of kilograms, providing extensive sample areas for analysis. The considerable sample sizes, along with large grain dimensions of typical olivine crystals, the kamacite and taenite domains within the matrix, and less-abundant phases such as sulfides or chromites, render pallasites highly suitable for assessing the potential of micro X-ray fluorescence (μ-XRF) analysis in studying correlated patterns between large-scale textures and chemical compositions.

The Esquel meteorite, weighing 0.7 tons, was discovered in Patagonia prior to 1951, and it exemplifies typical characteristics of an MG pallasite. A substantial slab of Esquel, measuring 68 × 31 × 0.5 cm and encompassing an area of approximately 1670 cm^2, was acquired by the National Museum of Natural Science (Taichung, Taiwan; NMNS000906-P003283). This study introduces distinctive chemical, textural, mineralogical, and microstructural insights into the Esquel pallasite, employing an innovative μ-XRF analysis. The objectives of this investigation were to present novel data regarding this renowned pallasite and propose a potential scenario concerning its origin.

MATERIALS AND METHODS

The Esquel Pallasite

The Esquel meteorite was discovered near the town of Esquel, situated in the northwest region of Chubut Province, Argentina in 1951. The specimen (measuring 68 × 31 × 0.5 cm) examined in this study is a fragment of Esquel collected by the National Museum of Natural Science in 1992. This sample exhibits the characteristic texture of a pallasitic structure, showcasing fragmented olivine and clusters of olivine (Fig. 1). Esquel can be categorized into four distinct lithologies: (1) a "pallasitic" matrix comprising olivine fragments embedded within metallic material; (2) sizable olivine nodules (>5 cm) characterized by low metal contents; (3) solid metallic regions; and (4) areas predominantly featuring FeS and fine olivine (Ulff-Møller 1998).

Micro X-ray Fluorescence (μ-XRF) Analysis

The elemental distribution of Esquel was mapped using a M6 Tornado μ-XRF spectrometer (BrukerNano, Berlin, Germany). This instrument was equipped with an Rh tube (operating at 50 kV and 200 μA) in conjunction with policapillary optics and two XFlash® silicon drift detectors (with a resolution of <145 eV @ the Mn Kα line) featuring an active area of 800 × 600 mm. Mapping was performed over an area measuring 671 × 329 mm using a step size of 300 μm, resulting in a total of 32,453,989 pixels in an image. Given the instrument's beam size of approximately 100 μm, the pixel dwell-time was established at 20 ms, leading to an overall measurement time of approximately 11 h (inclusive of operational procedures, totaling approximately 16 h).

RESULTS AND DISCUSSION

Mineralogical Characteristics of the Esquel Pallasite

Figures 2, 3, and 4 depict μ-XRF imaging outcomes, revealing the primary elements within the sample. Imaging was conducted with a 300-μm step between individual measurements, given a spot size of 100 μm. The color intensity of each element image corresponds to the spectral signal's intensity. Higher color intensities indicate greater signals for that specific element compared to the surrounding area. This allowed establishment of correlations between different elements based on their presence, abundance, and comparisons to other elements. Such correlations aided in further mineralogical interpretations by observing the coexistence or absence of elements and their relative concentrations.

The most abundant elements identified in

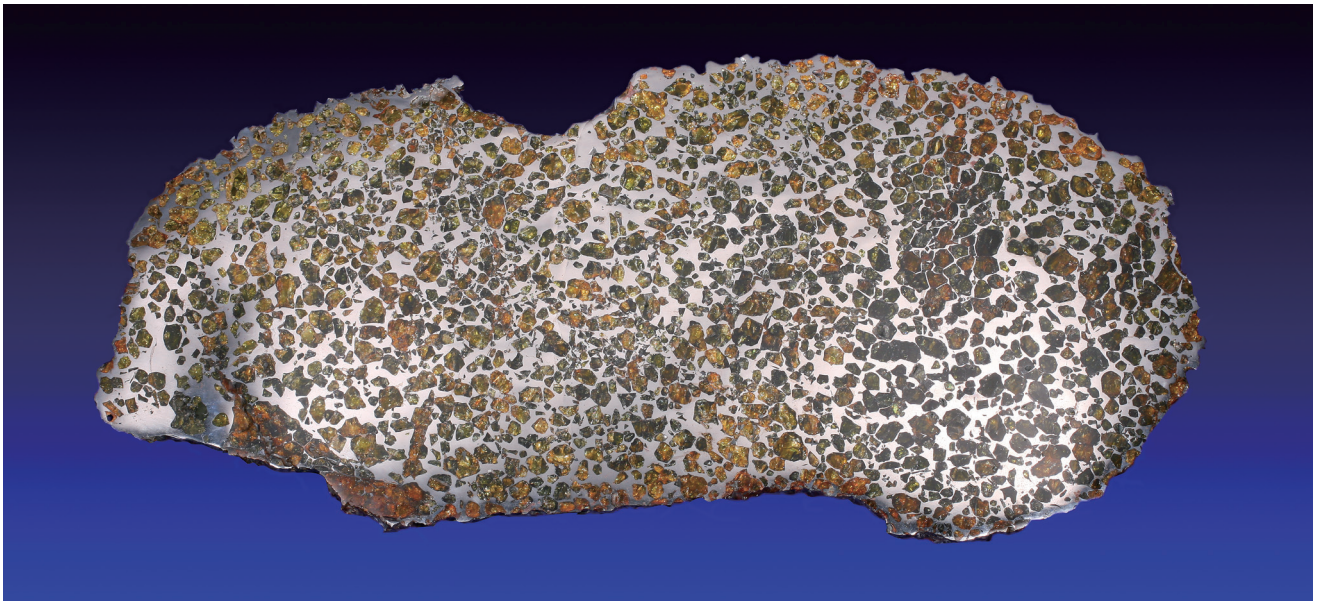

Fig. 1. This 68-cm-long section of the Esquel Main-Group pallasite was obtained by the National Museum of Natural Science. Approximately 80% of the surface displays characteristic pallasitic material, featuring angular olivine fragments embedded in metal. The remaining portion comprises two polycrystalline olivine aggregates, each measuring ~15 cm in length, exhibiting signs of disintegration into angular olivine fragments. Olivine aggregates can be observed in the middle of the right half and the lower section of the left half of the specimen.

the Esquel pallasite by the μ-XRF analysis were Si, Mg, Fe, and Ni followed by P, S, and Cr. Additional characteristic peaks of very low intensity of other elements, i.e., Mn, Cu, Zn, and As, were detected. Distribution maps of major and trace elements are shown in Figs. 2, 3, and 4. In each element-distribution map, the brightness of each pixel reflects the intensity of the fluorescence signal of that element with respect to the surrounding area.

The meteorite exhibited two primary mineral domains, distinguished by the correlation of Si in one and Ni with Fe in the other. These distinctions align with the olivine and (Fe, Ni) metal assemblages, specifically taenite and kamacite, respectively. This categorization was supported by the various intensities of green observed in the Ni map (see Fig. 2), consistent with the higher Ni content in taenite compared to kamacite.

Furthermore, the presence and distributions of S, Cr, and Ca respectively corresponded with troilite (FeS), chromite ($FeCr_2O_4$), and phosphates (such as merrillite ($Ca_{18}Na_2Mg_2(PO_4)_2$ and stanfieldite ($Ca_3Mg_3(PO_4)_4$)). The simultaneous occurrence and spatial distributions of Fe and P are indicative of phosphide schreibersite ($(Fe, Ni)_3P$). The element map of P exhibited extremely subtle variations in certain regions, making it challenging to visualize; hence, those data are not displayed.

The mapping of each elemental image was defined using ImageJ software (National Institutes of Health, Bethesda, MD, USA) for subsequent analyses. Derived areas were translated into components of individual minerals, indicating phase abundances as follows: olivine (58%), kamacite (26%), taenite (10%), troilite (1.7%), schreibersite (1.5%), chromite (0.7%), and phosphates (1.5%).

Implications for Pallasite Formation

The origins of pallasites have remained enigmatic since their initial description in the late 18th century (referred to as the 'pallasite problem', Wahl 1965), primarily due to the presence of two phases (metal and silicates) with different densities that should theoretically have segregated under gravitational forces, especially when the metal was in a liquid state. Until recently, it was a prevalently believed that pallasites originated from the core-mantle boundary region of a planetesimal (e.g., Wasson and Choi 2003; Boesenberg *et al*. 2012). Although impact processes were implicated in various theories as to their origin (Boesenberg *et al*. 2012), compelling evidence supporting the current two-

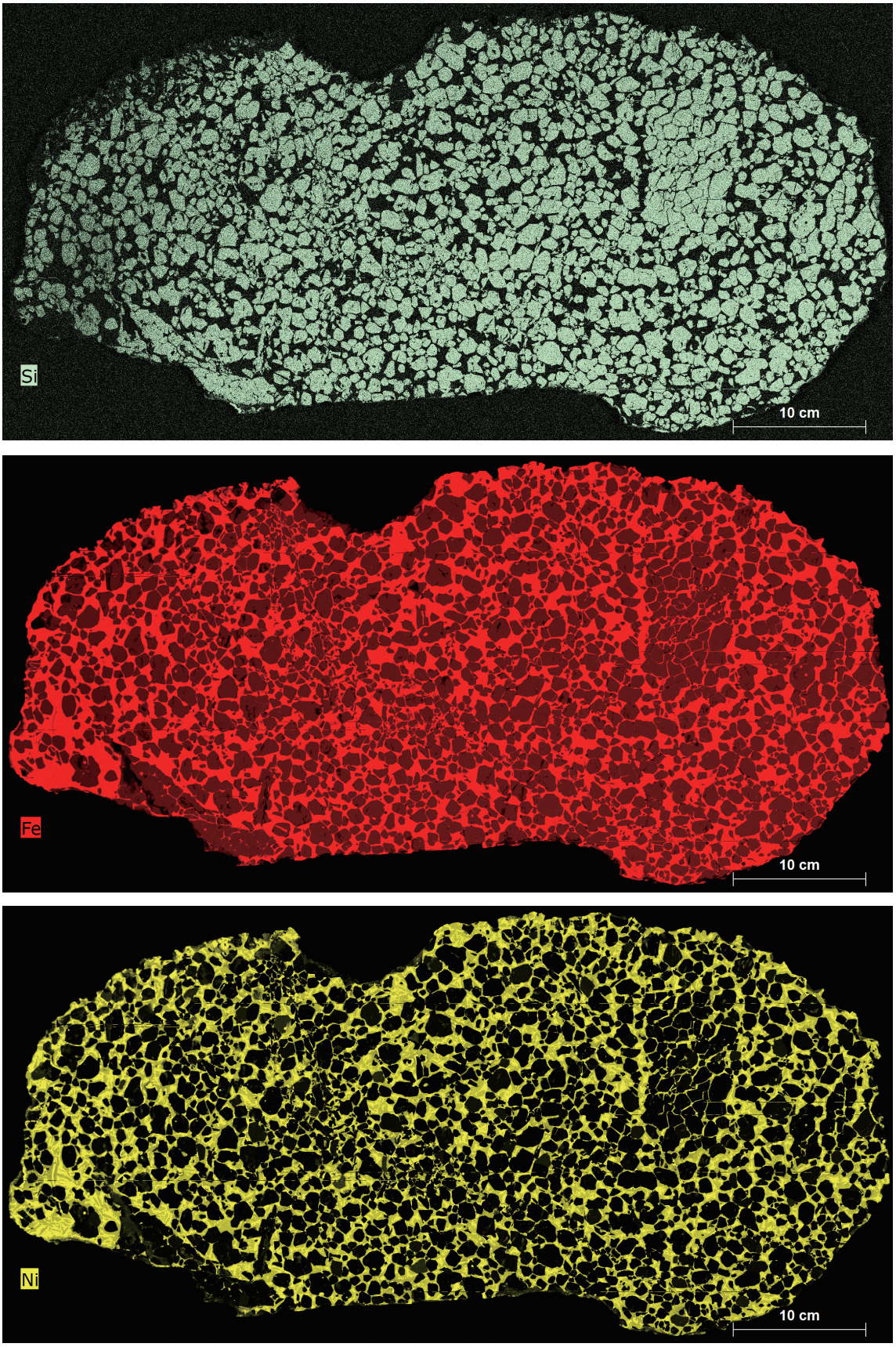

Fig. 2. Element distribution maps of Si, Fe, and Ni for the Esquel pallasite.

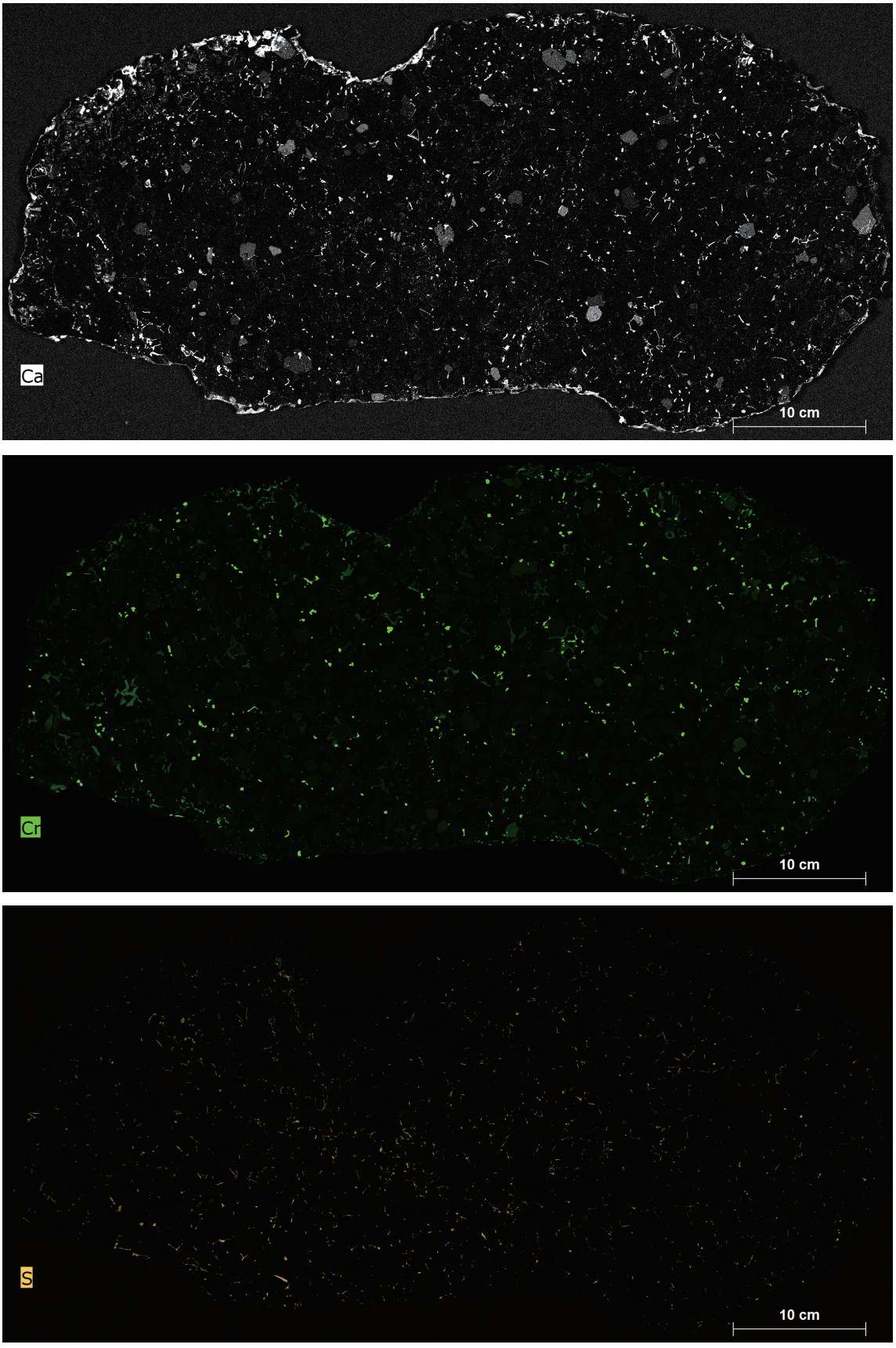

Fig. 3. Element distribution maps of Ca, Cr, and S for the Esquel pallasite.

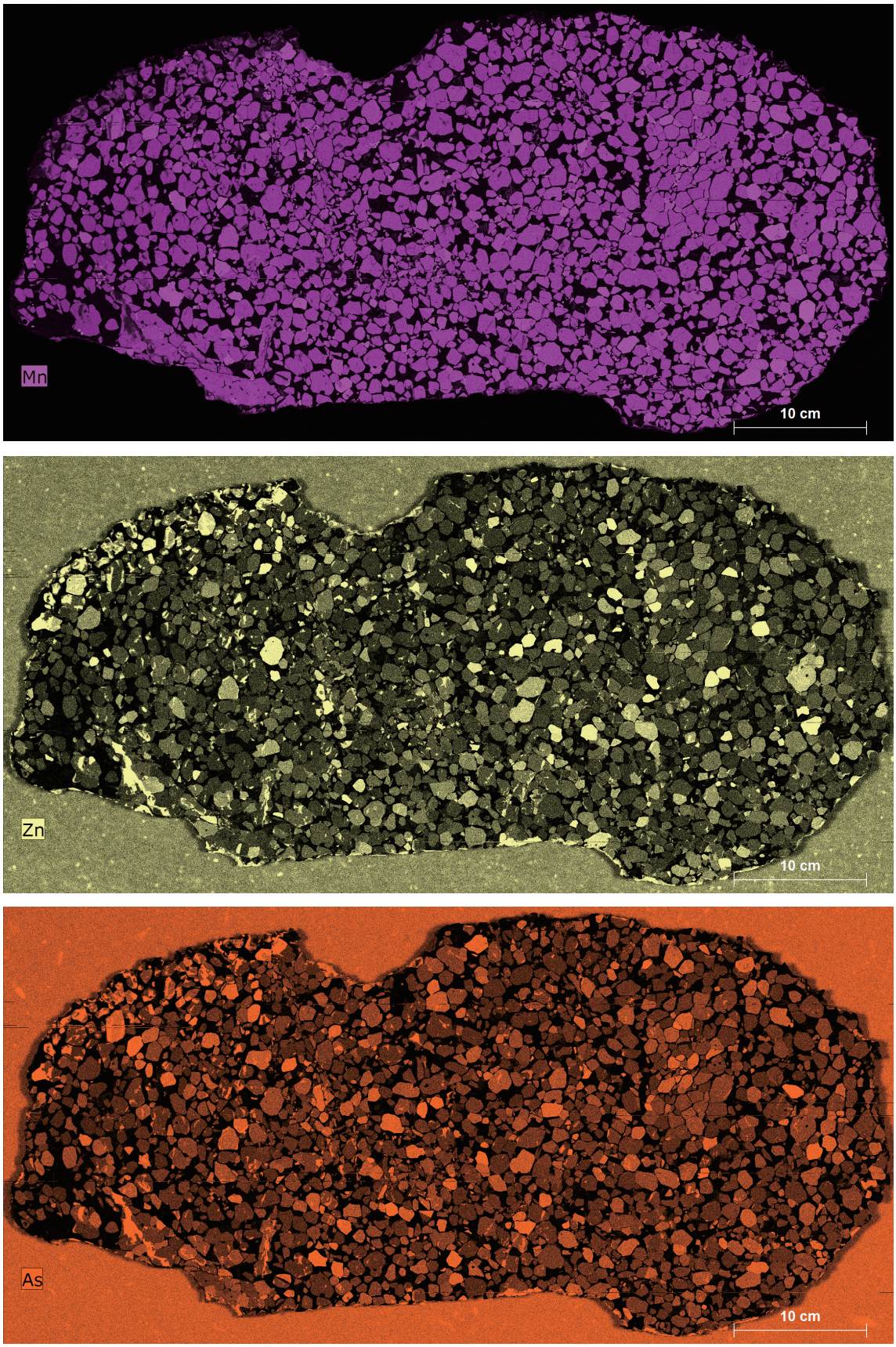

Fig. 4. Element distribution maps of Mn, Zn, and As for the Esquel pallasite.

body collision model has only surfaced in recent years. Consequently, the origins of pallasites remain a topic of controversy.

Nevertheless, concentrations of numerous trace elements, such as Ti, V, Cr, and Ni, underwent significant variations within olivines during the mixing and cooling process with metals (e.g., Hsu *et al*. 2003). Mapping these trace elements within olivine and metals could offer insights into the early crystallization history, aiding in unraveling their origins.

Figure 4 illustrates the distribution of Mn, corresponding to the distribution of Si, indicating the presence of Mn within olivines, with certain grains exhibiting higher Mn contents. However, clear correlations were not evident between the distribution of Mn and the shape of olivine, which can be formed through various processes during pallasite formation. One of the distinctive features in Esquel is the presence of olivine aggregates. These aggregates consist of euhedral olivines that primarily break along grain boundaries as metal infiltrated the cluster, gradually reaching a form of textural equilibrium (see Fig 1; the central area of the right half of the specimen). These aggregates likely represent well-preserved samples from different mantle regions of pallasite parent bodies (Scott 1977; Walte and Golabek 2022). However, no systematic distributions of Mn were observed within the domain of olivine aggregates.

Figures 4 also depicts distributions of Zn and As. Both elements are predominantly associated with olivines. However, the distribution patterns of As and Zn contents within olivine are inconsistent, suggesting differing diffusion behaviors during pallasite formation. Notably, the upper left olivine crystals in the specimen exhibit uneven Zn and As contents, with some displaying a vein-like distribution. Furthermore, on the lower left side of the specimen, regions rich in As and Zn traverse through the olivine aggregates in vein-like structures. These areas, abundant in Zn and As, are likely correlated with olivine alterations, prompting further investigation into the mineral phases formed within these veins.

While the elemental distributions outlined in this study present enigmatic patterns owing to the spatial scale of variations, integration of trace elements into olivine and significant insights into pallasite formation have been gleaned by applying this mapping methodology. Further exploration of these trace element characteristics, possibly at smaller scales and as part of a comparative analysis between olivine extracted from pallasites, chondrites, and primitive achondrites, could unveil the proportion of olivine originating from magmatic processes. Such an investigation might shed light on the relevant environments pertinent to the origin of pallasite olivine.

CONCLUSIONS

This study aimed to introduce a novel approach utilizing μ-XRF to obtain chemical insights and microstructural details of the Esquel pallasite. The minerals—olivine, kamacite, taenite, schreibersite, troilite, chromite, and Ca-rich phosphates—were identifiable and visually represented within the slab, offering valuable indications regarding their origins and impact histories. The μ-XRF technique serves as a completely non-invasive, non-destructive method for high-resolution mapping of spatial distributions of specific elements and crystalline phases within millimeter-sized heterogeneous samples. Ultimately, the analytical methodology outlined in this study is expected to be applicable for assessing other rare meteorites.

ACKNOWLEDGEMENTS

I wish to extend my heartfelt appreciation to Dean Tech Co., Ltd. (New Taipei City, Taiwan) for their invaluable support in instrumentation and data analysis during the course of this research.

REFERENCES

Boesenberg, J.S., J.S. Delaney, and R.H. Hewins. 2012. A petrological and chemical reexamination of Main Group pallasite formation. Geochim. Cosmochim. Acta 89: 134-158.

Hsu, W. 2003. Minor element zoning and trace element geochemistry of pallasites. Meteorit. Planet. Sci. 38: 1217-1241.

Miyamoto, M. 1997. Chemical zoning of olivine in several pallasites. J. Geophys. Res. Planets 102: 21613-21618.

Norton, O.R. and L.A. Chitwood. 2008. Field guide to

meteors and meteorites. Springer, London.
Scott, E.R. 1977. Formation of olivine-metal textures in pallasite meteorites. Geochim. Cosmochim. Acta 41(6): 693-710.
Ulff-Møller, F., B.G. Choi, A.E. Rubin, J. Tran, and J.T. Wasson. 1998. Paucity of sulfide in a large slab of Esquel: new perspectives on pallasite formation. Meteorit. Planet. Sci. 33(2): 221-227.
Walte, N.P. and G.J. Golabek. 2022. Olivine aggregates reveal a complex collisional history of the Main Group pallasite parent body. Meteorit. Planet. Sci. 57(5): 1098-1115.
Wasson, J.T. and B.G. Choi. 2003. Main-Group pallasites: chemical composition, relationship to Iiiab irons, and origin. Geochim. Cosmochim. Acta 67(16): 3079-3096.
Weisberg, M.K., T.J. McCoy, and A.N. Krot. 2006. Systematics and evaluation of meteorite classification. In D.S. Lauretta and H.Y. McSween Jr. (eds.). Meteorites and the early solar system II. University of Arizona Press, Tucson, AZ. pp. 19-52.
Weisberg, M.K., J.S. Boesenberg, G. Kozhushko, M. Prinz, R.N. Clayton, and T.K. Mayeda. 1995. Eh3 and El3 chondrites: a petrologic-oxygen isotopic study. Lunar Planet. Sci. Conf. 26: 1481-1482.
Yang, J., J.I. Goldstein, and E.R. Scott. 2010. Main-Group pallasites: thermal history, relationship to Iiiab irons, and origin. Geochim. Cosmochim. Acta 74(15): 4471-4492.

利用微區X光螢光技術分析Esquel橄欖隕鐵中的元素分布

陳君榮

國立自然科學博物館地質學組

大型Esquel橄欖隕鐵切片 (68 × 31 × 0.5 公分)首次以微區X光螢光分析技術來進行研究。 Esquel橄欖隕鐵元素分布圖顯示：（1）礦物組成包含橄欖石（58%）、鐵紋石（26%）、鎳紋石（10%）、隕硫鐵（1.7% ）、隕磷鐵鎳礦（1.5%）、鉻鐵礦（0.7%），以及磷酸鹽類（1.6%；隕磷鈉鎂鈣石或隕磷鎂鈣石）；（2）橄欖石在錳、鋅及砷等微量元素之含量有明顯差異。 角狀橄欖石及橄欖石聚集體的同時存在，以及橄欖石中所含錳、鋅及砷等微量元素的變化，顯示Esquel橄欖隕鐵是經由多個階段所形成，且過程中可能包含一次或多次的撞擊事件。

關鍵詞：橄欖隕鐵、Esquel、微區X光螢光光譜分析、元素分布。